Article

https://doi.org/10.1038/s41567-023-02139-8

Many-body chemical reactions in a quantum degenerate gas

Received: 30 November 2022

Zhendong Zhang 📵 , Shu Nagata, Kai-Xuan Yao 🛈 & Cheng Chin 🗅 🖂

Accepted: 21 June 2023

Published online: 24 July 2023



Chemical reactions in the quantum degenerate regime are described by the mixing of matter-wave fields. In many-body reactions involving bosonic reactants and products, such as coupled atomic and molecular Bose-Einstein condensates, quantum coherence and bosonic enhancement are key features of the reaction dynamics. However, the observation of these many-body phenomena, also known as 'superchemistry', has been elusive so far. Here we report the observation of coherent and collective reactive coupling between Bose-condensed atoms and molecules near a Feshbach resonance. Starting from an atomic condensate, the reaction begins with the rapid formation of molecules, followed by oscillations of their populations during the equilibration process. We observe faster oscillations in samples with higher densities, indicating bosonic enhancement. We present a quantum field model that captures the dynamics well and allows us to identify three-body recombination as the dominant reaction process. Our findings deepen our understanding of quantum many-body chemistry and offer insights into the control of chemical reactions at quantum degeneracy.

Ultracold atoms and molecules form an ideal platform towards controlling chemical reactions at the level of single internal and external quantum states. Ultracold molecules can be prepared in an individual internal state by, for example, the magnetoassociation¹ and photoassociation² of ultracold atoms and direct laser cooling³. The external motion of molecules can be constrained by loading them into optical lattices⁴ or tweezers⁵. These experiments lead to the realization of state-to-state ultracold chemistry⁶⁻⁸.

A number of experiments on cold molecules have reached the regime of quantum degeneracy, which promise new forms of molecular quantum matter and reaction dynamics. For instance, molecular Bose-Einstein condensates (BECs) formed in atomic Fermi gases have stimulated tremendous interest in the BEC-to-Bardeen-Cooper-Schrieffer crossover 9,10. Degenerate fermionic molecules are created by the magnetoassociation of bosonic and fermionic atoms and optical transitions to the lowest rovibrational state¹¹. Here quantum degeneracy suppresses chemical reactions due to the fermion antibunching effect¹¹.

Recently, molecular BECs have been realized based on atomic BECs near a Feshbach resonance¹². The reactive coupling between condensed atoms and molecules promises a new regime of quantum chemistry, dubbed 'quantum superchemistry', which highlights the coherent coupling of macroscopic matter waves and Bose stimulation of the reaction process^{13,14}. A key feature of this coherence is the collective oscillations between the reactant and product populations. Because of Bose statistics, the collective enhancement of reaction dynamics is anticipated near a Feshbach resonance¹⁵.

At quantum degeneracy, the reaction dynamics fundamentally arise from the mixing of the matter-wave fields of the reactants and products. For instance, consider Feshbach coupling that converts two atoms into one molecule and vice versa, described by the chemical equation: $A + A \leftrightarrow A_2$. In a quantum gas, the reaction is described by the many-body Hamiltonian with the reaction order $\alpha = 3$:

$$\hat{H} = \varepsilon_{\mathrm{m}} \hat{\psi}_{\mathrm{m}}^{\dagger} \hat{\psi}_{\mathrm{m}} + g_2 \hat{\psi}_{\mathrm{m}}^{\dagger} \hat{\psi}_{\mathrm{a}}^2 + g_2 \hat{\psi}_{\mathrm{a}}^{\dagger 2} \hat{\psi}_{\mathrm{m}}, \tag{1}$$

where $\hat{\psi}_a(\hat{\psi}_m)$ is the atomic (molecular) field operator, g_2 is the Feshbach coupling strength and $\varepsilon_{\rm m}$ is the energy of one bare molecule relative to two bare atoms. Here we define the reaction order α as the maximum number of field operators in reaction terms.

Another prominent example that couples ultracold atoms and molecules is three-body recombination, where three colliding atoms are converted into a diatomic molecule and another atom,

The James Franck Institute, Enrico Fermi Institute and Department of Physics, University of Chicago, Chicago, IL, USA. 🖂 e-mail: cchin@uchicago.edu

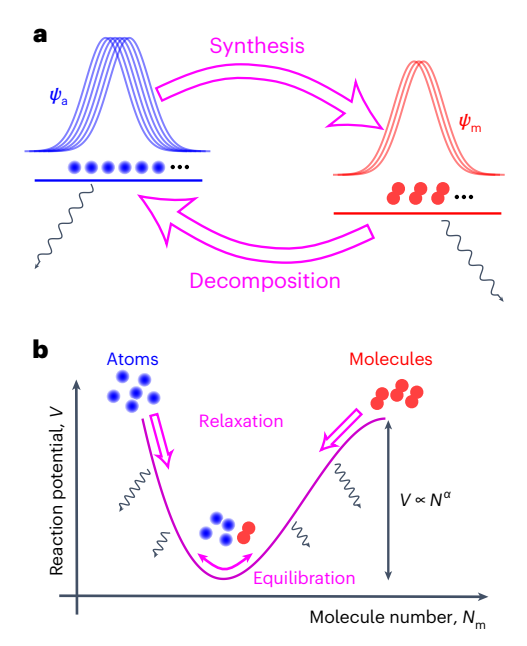


Fig. 1| **Reactive coupling between atomic and molecular quantum fields. a**, Bose-condensed atoms described by a single wavefunction ψ_a are coupled to molecules condensed in state ψ_m . The coupling synthesizes and decomposes molecules. The wavy lines represent dissipation. **b**, We introduce a reaction potential V to describe the many-body dynamics of the atomic and molecular fields. A pure sample of atoms or molecules first relaxes towards a lower potential and then equilibrates near the potential minimum. Due to bosonic stimulation, the potential scales as $V \propto N^\alpha$, where N is the total particle number and α is the reaction order, as shown in the main text.

and vice versa. This process is described by the chemical equation $A+A+A\leftrightarrow A_2+A$. At quantum degeneracy, the recombination process can resonantly couple atomic and molecular fields as

$$\hat{h}_{3} = g_{3} \hat{\psi}_{m}^{\dagger} \hat{\psi}_{a}^{\dagger} \hat{\psi}_{a}^{3} + g_{3} \hat{\psi}_{a}^{\dagger 3} \hat{\psi}_{a} \hat{\psi}_{m}, \tag{2}$$

where g_3 is the recombination coupling strength. Here the reaction order is $\alpha = 5$.

To understand the dynamics of the coupled quantum fields, we present the following picture. We show that the molecular population $\hat{N}_m = \hat{\psi}_m^\dagger \hat{\psi}_m$ follows the form of an 'energy conservation' law as

$$\frac{\hbar^2}{2}\dot{\hat{N}}_{\rm m}^2 + V(\hat{N}_{\rm m}) = {\rm const.},\tag{3}$$

where $\hbar^2 \dot{\hat{N}}_{\rm m}^2/2$ resembles the kinetic energy and we introduce the many-body reaction potential $\hat{V} = [\hat{N}_{\rm m}, \hat{H}]^2/2 + {\rm const.}$ (Supplementary Information), which connects the reactants and products. In this picture, the system tends towards a lower potential. Quantum fluctuations of the nonlinear field coupling, however, can effectively damp the dynamics of the populations 16,17 . In experiments, damping can also come from inelastic scattering and coupling to a thermal field. Thus, one expects that the system first relaxes towards the potential minimum, and then equilibrates near the minimum with small-amplitude coherent oscillations (Fig. 1). In the thermodynamic limit with total particle number $N\gg 1$, the reaction potential and oscillation frequency near the minimum scale with the particle number as $V\propto N^{\alpha}$ and $\omega_0 \propto N^{(\alpha/2)-1}$. The dependence on the particle number signals the bosonic enhancement of the reaction dynamics 13,16 .

In this paper, we report the observation of coherent and Bose-stimulated reactions between Bose-condensed Cs atoms and

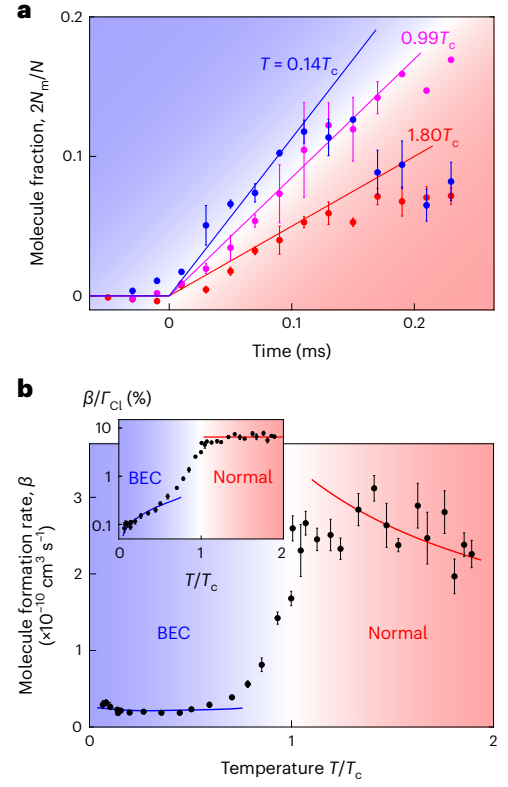


Fig. 2| **Comparison of molecule formation rate in classical and quantum degenerate regimes. a**, Dynamics of molecule formation in an atomic gas after quenching the magnetic field 3(2) mG above the Feshbach resonance at B_0 = 19.849(2) G. The solid lines are fits to the data in the initial growth stage for the extraction of molecule formation rate $\dot{N}_{\rm m}$. **b**, Extracted molecule formation rate coefficient β above and below the critical temperature $T_{\rm c}$. The red line is a fit to the data based on the classical kinetic theory prediction β = $b_{\rm cl} \Gamma_{\rm Cl}$, from which we obtain the classical branching ratio $b_{\rm cl}$ = 7(1)% (see the main text). The blue line fits the data in the quantum regime with β = $b_{\rm cl} \Gamma_{\rm cl}$, which gives the quantum branching ratio $b_{\rm q}$ = 3.9(3)% (see the main text). The inset shows the rate coefficient normalized to the classical gas expectation $\Gamma_{\rm Cl}$. In **a**, the error bars represent one standard deviation of the mean, estimated from 4–8 measurements. In **b**, the error bars represent 95% confidence intervals of the mean.

 Cs_2 molecules near an atomic Feshbach resonance. The reaction is initiated by tuning the magnetic field near a narrow g-wave Feshbach resonance, which couples scattering atoms and diatomic Feshbach molecules in a single high-lying rovibrational state bounded by van der Waals potential (Methods). Near the resonance, atomic and molecular populations quickly relax towards a dynamical equilibrium, followed by coherent oscillations between atoms and molecules in the equilibration process. We show that the oscillation frequency strongly depends on the particle number. From the dependence, we conclude that three-body recombination is the dominant reaction process that couples the atomic and molecular fields near the Feshbach resonance.

Our experiment starts with an ultracold Bose gas of 6×10^3 to 5×10^5 caesium atoms in an optical trap. The atoms can form a pure BEC either in a three-dimensional harmonic potential or a two-dimensional (2D) square well potential¹⁸. We induce the reaction by switching the magnetic field near the g-wave Feshbach resonance, which can convert an atomic BEC into a molecular BEC¹². We determine the resonance position B_0 = 19.849(2) G, resonance width ΔB = 8.3(5) mG and relative magnetic moment $\delta \mu$ = $h \times 0.76(3)$ MHz G⁻¹, where h is the Planck constant, from the measurements of molecular binding energy $\varepsilon_m \approx \delta \mu (B - B_0)$ and the scattering length (Methods). After the reaction, we decouple

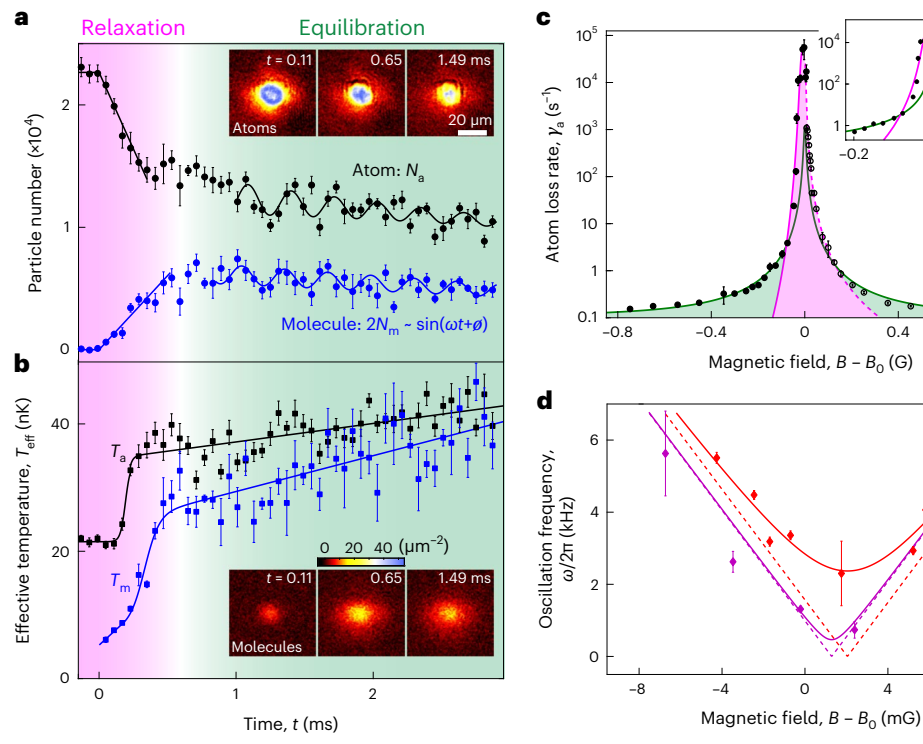


Fig. 3 | **Coherent reaction dynamics in quantum gases of atoms and molecules across a Feshbach resonance. a**, Evolution of atomic and molecular populations in an atomic BEC after quenching the magnetic field 2(1) mG below the resonance. The solid lines are fits to capture the dynamics in relaxation and equilibration processes. **b**, Effective temperatures determined from time-of-flight measurements of the atoms and molecules at the same field. The solid lines are guides to the eye. The insets in **a** and **b** show the sample images of atoms and molecules after the time of flight (Methods). **c**, Loss rate of atoms immediately after the quench. The solid (empty) circles represent samples prepared below (above) the resonance. The green line is a Lorentzian fit with the centre at B_0 and width ΔB . The magenta solid (dashed) line is a fit near and below (above) the resonance based on $\gamma_a = \gamma_0/[1 + |(B - B_0)/\delta B|^{\epsilon \pm}]$ (see the main text), from which

we obtain the exponent ϵ_- = 6(2) (ϵ_+ = 2.9(4)) below (above) the resonance. The inset shows a zoomed-in view near the resonance. **d**, Oscillation frequency of molecular populations from atomic samples at mean BEC density of 2.9 × 10¹³ cm⁻³ and BEC fraction of 80% (red) and 60% (purple). The solid lines are empirical fits based on $\hbar\omega = \sqrt{\delta\mu^2(B-B_{\rm m})^2 + \hbar^2\omega_0^2}$, where $B_{\rm m}$ and ω_0 are fitting parameters. The values of $B_{\rm m}$ from the fits are consistent with the resonance position B_0 within our measurement uncertainty. The dashed lines are the asymptotes $\hbar\omega = |\delta\mu(B-B_{\rm m})|$. Data in **a** and **b** are averages of 3–4 measurements, and the error bars represent one standard deviation of the mean. Data in **c** and **d** are obtained from the fits (Methods), and the error bars represent 95% confidence intervals.

the atoms and molecules by quickly tuning the magnetic field far off the resonance and image each independently¹².

To show that chemical reactions follow different rules in a degenerate quantum gas versus a normal gas, we compare the molecule production rate for samples prepared above and below the BEC critical temperature $T_{\rm c}$. To describe the molecular formation dynamics in the transition from the classical to quantum degenerate regime, we present the molecule production rate in terms of $\beta = \dot{N}_m/N_0 n_0$ right after the magnetic-field quench, where N_0 and n_0 are the initial total atom number and mean atomic density, respectively (Fig. 2).

The measured molecule formation rate shows a distinct behaviour in the two regimes. In a thermal gas with temperature $T > T_c$, the molecule formation rate is $\beta = b_{Cl} \Gamma_{Cl}$, where Γ_{Cl} is the classical atomic collision rate coefficient and b_{Cl} is the classical branching ratio that represents the probability of molecule formation from each collision event. Near the resonance, the collision rate coefficient is unitarity limited as $\Gamma_{Cl} = 8h^2(\pi^3 m^3 k_B T)^{-1/2}$ (ref. 19), where m is the atomic mass and k_B is the Boltzmann constant. Our measurement in the thermal regime is consistent with $T^{-1/2}$ scaling. From the fit, we extract the branching ratio $b_{Cl} = 7(1)\%$ (Fig. 2b).

Entering the quantum degenerate regime $T < T_c$, we observe a steep drop in the rate coefficient (Fig. 2b). At low temperatures, we model the rate coefficient as $\beta = b_Q \Gamma_Q$, where b_Q and $\Gamma_Q = 4\sqrt{3}(h/m)(6\pi^5 n)^{-1/3}$ are the branching ratio and rate coefficient predicted by the universal

theory in the quantum regime, respectively 20,21 . The model fits the measurement well, and we extract the branching ratio to be $b_{\rm Q}$ = 3.9(3)%. The sharp transition of the molecule formation rate around critical temperature $T_{\rm c}$ indicates different laws in the classical and quantum degenerate regimes. The suppression of the reaction rate in atomic BECs can be attributed to the suppression of correlations in the condensed phase 22 , as well as strong interactions between atoms and molecules across the Feshbach resonance.

A close examination of the molecule formation dynamics in atomic BECs reveals additional interesting features of quantum many-body reactions. To understand the underlying reaction processes, we study the atom loss rate $\gamma_a = -\dot{N}_a/N_0$ right after switching the magnetic field, where N_a is the atom number (Fig. 3c). Far from the resonance $|B-B_0|\gg \Delta B$, atoms decay slowly and the loss rate follows a symmetric Lorentzian profile centred at the resonance $\gamma_a \propto (B-B_0)^{-2}$. We attribute the symmetric Lorentzian lineshape to the Feshbach coupling that off-resonantly couples two atoms to a molecule, and the molecule is lost when it collides with a third atom inelastically¹⁹.

Near the resonance, the loss rate greatly exceeds the expectation from the Lorentzian profile. This rapid atom loss only lasts for a few hundreds of microseconds and is accompanied with fast molecule production and heating of both atoms and molecules. We identify this fast process as the relaxation dynamics (Fig. 1b). To characterize the enhanced reaction rate, we fit the loss rate near the resonance as

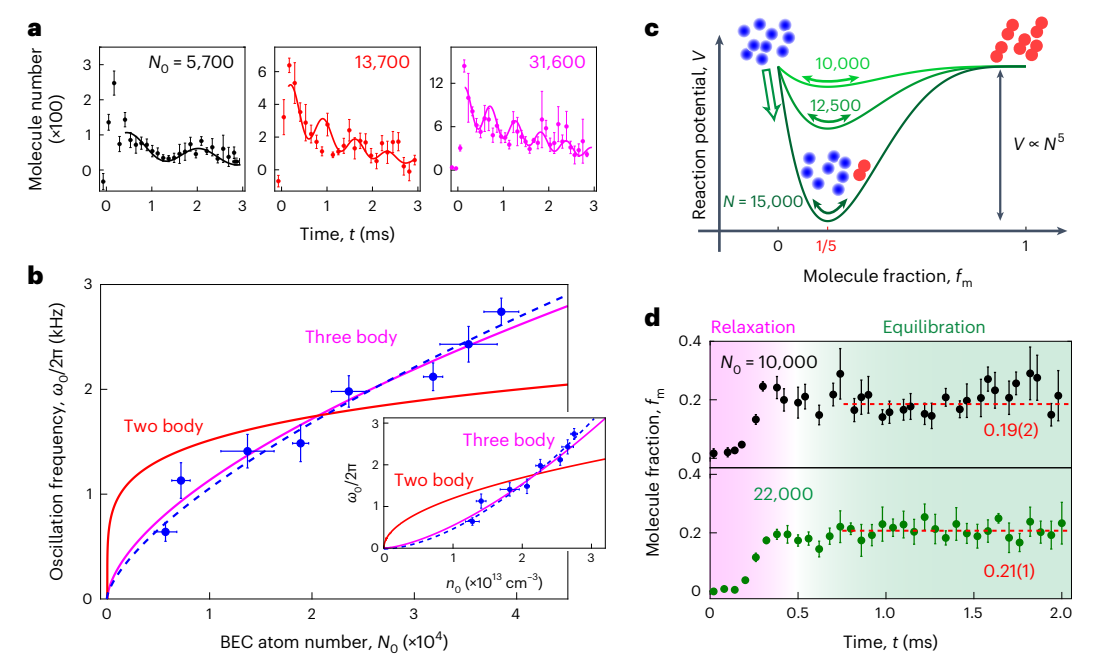


Fig. 4 | **Bose-enhanced atom-molecule reaction dynamics on Feshbach resonance. a**, Molecules formed in atomic BECs with different initial atom numbers N_0 following the magnetic field quench to 1(1) mG below the Feshbach resonance. The solid lines are fits to the data. **b**, Extracted oscillation frequencies for different initial atom numbers N_0 . The red (magenta) solid line is a power-law fit with exponent given by the two-body (three-body) model. The blue dashed line is a power-law fit with a free exponent, which yields the scaling $\omega_0 \propto N_0^{0.7(2)}$. In the inset, we show the frequency dependence on the mean atomic density n_0 and the associated fits that yield the scaling $\omega_0 \propto n_0^{1.7(4)}$. **c**, Reaction potential

 $V \equiv V_3 \approx -4g_3^2 N^3 f_{\rm m} (1-f_{\rm m})^4$ of the three-body process described in equation (2) for different total particle numbers N (green solid lines). In the thermodynamic limit $N \gg 1$, the minimum occurs at molecule fraction $f_{\rm m} \equiv 2N_{\rm m}/N = 1/5$. **d**, Evolution of molecule fraction $f_{\rm m}$ for different initial atom numbers N_0 . The mean molecule fractions in the equilibration phase $f_{\rm m} = 19(2)\%$ and $f_{\rm m} = 21(1)\%$ are consistent with the predicted minimum position of V_3 at $f_{\rm m} = 1/5$. Here the uncertainties represent 95% confidence intervals. Data in **a** and **d** are averages of 3–5 measurements and the error bars represent one standard deviation of the mean. The error bars in **b** represent 95% confidence intervals.

 $\gamma_a \propto [1+|(B-B_0)/\delta B|^{\epsilon_\pm}]^{-1}$ from which we extract the exponents $\epsilon_+ = 2.9(4)$ above the resonance and $\epsilon_- = 6(2)$ below the resonance. The exponents ϵ_\pm larger than 2 are consistent with the enhanced atom loss near the resonance beyond the Lorentzian profile.

The relaxation dynamics stem from three-body recombination, evidenced by the fast heating of both species in the relaxation phase (Fig. 3b)²³. In addition, the measured exponent ϵ_+ = 2.9(4) from the enhanced atom loss is consistent with the predicted value of 3.5 for three-body recombination near a narrow Feshbach resonance ^{24,25}. We attribute the even larger exponent ϵ_- = 6(2) below the resonance to the bosonic enhancement of the three-body process.

Following the relaxation, both atomic and molecular populations oscillate for several milliseconds before they slowly decay over a much longer timescale (Fig. 3a,b and Methods). The oscillation indicates a coherent coupling between the atomic and molecular fields, consistent with the equilibration dynamics near the reaction potential minimum (Fig. 1b). The frequency ω of oscillation depends on the magnetic field and is well fit to $\omega = \sqrt{\epsilon_m^2/\hbar^2 + \omega_0^2}$ (Fig. 3d). Far from the resonance, the frequency approaches the molecular binding energy $|\epsilon_m|$. On resonance with $\epsilon_m = 0$, the frequency $\omega = \omega_0$ is given by the collective reactive coupling between the atomic and molecular fields.

To demonstrate the many-body nature of the reactive coupling, we probe the atom–molecule oscillations right on the Feshbach resonance with different initial atom numbers N_0 and mean densities n_0 . After quenching the magnetic field, we observe that samples with higher populations and densities display faster oscillations (Fig. 4a). Fitting the data, we obtain the scaling $\omega_0 \propto N_0^{0.7(2)}$ and $\omega_0 \propto n_0^{1.7(4)}$ (Fig. 4b). Note that the two scalings are linked by $n_0 \propto N_0^{2/5}$ for BECs in a harmonic trap^{26–28}. The particle number dependence of the reactive

coupling supports the bosonic enhancement of the reaction process.

The scaling with respect to the particle number also reveals the underlying reaction mechanism. For the three-body recombination process described in equation (2), we derive the effective potential $V_3 = -g_3^2 N^5 f_{\rm m} (1-f_{\rm m})^4 + O(N^4)$, where $f_{\rm m} = 2N_{\rm m}/N$ is the molecule fraction, from which the resonant oscillation frequency is calculated to be $\omega_0 \propto N^{3/5}$ in a harmonic trap (Supplementary Information). For the two-body recombination process described in equation (1), the effective potential is $V_2 = -g_2^2 N^3 f_{\rm m} (1-f_{\rm m})^2 + O(N^2)$ which yields the scaling $\omega_0 \propto N^{1/5}$. Our measurement agrees well with the three-body model (Fig. 4b).

Moreover, we find that the molecule fraction oscillates at around 20(1)% in the equilibration phase, which is consistent with the minimum position of the reaction potential V_3 at $f_m = 1/5$ (Fig. 4c,d). The two-body Feshbach process, on the other hand, predicts a different minimum of V_2 at $f_m = 1/3$. We note that the total population decays over a timescale longer than 5 ms, and thus, our theory model can describe the coherent atom—molecule coupling that occurs at a few kilohertz. The overall population loss due to inelastic collisions can contribute to damping of the coherent oscillations.

To conclude, we observe collective many-body chemical reactions in an atomic BEC near a Feshbach resonance. The dynamics are well described by a quantum field model derived from three-body recombinations. In particular, the coherent oscillations of atomic and molecular fields in the equilibration phase support quantum coherence and Bose enhancement of the reaction process. The observation of coherent and collective chemical reactions in the quantum degenerate regime paves the way to explore the interplay between many-body physics and ultracold chemistry.

Online content

Any methods, additional references, Nature Portfolio reporting summaries, source data, extended data, supplementary information, acknowledgements, peer review information; details of author contributions and competing interests; and statements of data and code availability are available at https://doi.org/10.1038/s41567-023-02139-8.

References

- Köhler, T., Góral, K. & Julienne, P. S. Production of cold molecules via magnetically tunable Feshbach resonances. *Rev. Mod. Phys.* 78, 1311–1361 (2006).
- Jones, K. M., Tiesinga, E., Lett, P. D. & Julienne, P. S. Ultracold photoassociation spectroscopy: long-range molecules and atomic scattering. Rev. Mod. Phys. 78, 483–535 (2006).
- Shuman, E. S., Barry, J. F. & DeMille, D. Laser cooling of a diatomic molecule. Nature 467, 820–823 (2010).
- Yan, B. et al. Observation of dipolar spin-exchange interactions with lattice-confined polar molecules. *Nature* **501**, 521–525 (2013).
- Cairncross, W. B. et al. Assembly of a rovibrational ground state molecule in an optical tweezer. *Phys. Rev. Lett.* 126, 123402 (2021).
- Wolf, J. et al. State-to-state chemistry for three-body recombination in an ultracold rubidium gas. Science 358, 921–924 (2017).
- Rui, J. et al. Controlled state-to-state atom-exchange reaction in an ultracold atom-dimer mixture. Nat. Phys. 13, 699-703 (2017).
- Liu, Y. et al. Precision test of statistical dynamics with state-to-state ultracold chemistry. *Nature* 593, 379–384 (2021).
- Chen, Q., Stajic, J., Tan, S. & Levin, K. BCS-BEC crossover: from high temperature superconductors to ultracold superfluids. *Phys. Rep.* 412, 1–88 (2005).
- Giorgini, S., Pitaevskii, L. P. & Stringari, S. Theory of ultracold atomic Fermi gases. Rev. Mod. Phys. 80, 1215–1274 (2008).
- 11. Marco, L. D. et al. A degenerate Fermi gas of polar molecules. *Science* **363**, 853–856 (2019).
- Zhang, Z., Chen, L., Yao, K.-X. & Chin, C. Transition from an atomic to a molecular Bose–Einstein condensate. *Nature* 592, 708–711 (2021).
- Heinzen, D. J., Wynar, R., Drummond, P. D. & Kheruntsyan, K. V. Superchemistry: dynamics of coupled atomic and molecular Bose-Einstein condensates. *Phys. Rev. Lett.* 84, 5029–5033 (2000).
- Malla, R. K., Chernyak, V. Y., Sun, C. & Sinitsyn, N. A. Coherent reaction between molecular and atomic Bose-Einstein condensates: integrable model. *Phys. Rev. Lett.* 129, 033201 (2022).

- Moore, M. G. & Vardi, A. Bose-enhanced chemistry: amplification of selectivity in the dissociation of molecular Bose-Einstein condensates. *Phys. Rev. Lett.* 88, 160402 (2002).
- Vardi, A., Yurovsky, V. A. & Anglin, J. R. Quantum effects on the dynamics of a two-mode atom-molecule Bose-Einstein condensate. *Phys. Rev. A* 64, 063611 (2001).
- 17. Richter, F. et al. Ultracold chemistry and its reaction kinetics. *New J. Phys.* **17**, 055005 (2015).
- Clark, L. W., Gaj, A., Feng, L. & Chin, C. Collective emission of matter-wave jets from driven Bose–Einstein condensates. *Nature* 551, 356–359 (2017).
- Chin, C., Grimm, R., Julienne, P. & Tiesinga, E. Feshbach resonances in ultracold gases. Rev. Mod. Phys. 82, 1225–1286 (2010).
- Makotyn, P., Klauss, C. E., Goldberger, D. L., Cornell, E. A. & Jin, D. S. Universal dynamics of a degenerate unitary Bose gas. *Nat. Phys.* 10, 116–119 (2014).
- 21. Eismann, U. et al. Universal loss dynamics in a unitary Bose gas. *Phys. Rev. X* **6**, 021025 (2016).
- 22. Burt, E. A. et al. Coherence, correlations, and collisions: what one learns about Bose-Einstein condensates from their decay. *Phys. Rev. Lett.* **79**, 337 (1997).
- Greene, C. H., Giannakeas, P. & Pérez-Ríos, J. Universal few-body physics and cluster formation. Rev. Mod. Phys. 89, 035006 (2017).
- 24. Petrov, D. S. Three-boson problem near a narrow Feshbach resonance. *Phys. Rev. Lett.* **93**, 143201 (2004).
- Chin, C. & Grimm, R. Thermal equilibrium and efficient evaporation of an ultracold atom-molecule mixture. *Phys. Rev. A* 69, 033612 (2004).
- 26. Pethick, C. J. & Smith, H. Bose–Einstein Condensation in Dilute Gases (Cambridge Univ. Press, 2008).
- 27. Hung, C.-L. In Situ Probing of Two-Dimensional Quantum Gases (The Univ. Chicago, 2011).
- Liu, B., Fu, L.-B. & Liu, J. Shapiro-like resonance in ultracold molecule production via an oscillating magnetic field. *Phys. Rev.* A 81, 013602 (2010).

Publisher's note Springer Nature remains neutral with regard to jurisdictional claims in published maps and institutional affiliations.

Springer Nature or its licensor (e.g. a society or other partner) holds exclusive rights to this article under a publishing agreement with the author(s) or other rightsholder(s); author self-archiving of the accepted manuscript version of this article is solely governed by the terms of such publishing agreement and applicable law.

© The Author(s), under exclusive licence to Springer Nature Limited 2023

Methods

Experimental procedure

Our experiment starts with an ultracold Bose gas of 6,000 to 470,000 atoms of 133 Cs at a temperature of 2–232 nK in a three-dimensional harmonic trap. We tune the temperature and atom number by changing the trap depth at the end of the evaporation process²⁹. The harmonic trap frequencies range from $(\omega_x, \omega_y, \omega_z) = 2\pi \times (24, 13, 74)$ to $2\pi \times (36, 15, 91)$ Hz. The atoms are polarized into the hyperfine ground state $|F=3, m_F=3\rangle$, where F and m_F are the quantum numbers for the total spin and its projection along the magnetic-field direction, respectively. The narrow g-wave Feshbach resonance couples Cs atoms into Cs₂ molecules at $|f=3, m_F=4; l=4, m_l=2\rangle$, where f and l represent the quantum numbers for the sum of the spins of two individual atoms and the orbital angular momentum of a molecule, respectively, and m_f and m_l are the projections of f and l along the magnetic-field direction, respectively³⁰.

To induce the molecule formation dynamics, we quench the magnetic field close to the resonance position B_0 from 19.5 G where the samples are prepared. After holding for variable times, we switch the field back to either 19.50 G or 17.17 G to decouple atoms and molecules. We can image the remaining atoms at this field by absorption imaging. We can also wait for the remaining atoms to fly away after a resonant light pulse and image the molecules by jumping the field up to 20.4 G to dissociate them into atoms and then image the atoms from the dissociation¹². For the atom loss measurements shown in Fig. 3c, BECs with ~40,000 atoms are transferred from the harmonic trap to a 2D flat-bottomed optical potential before we quench the field to different values near the resonance¹⁸. For the rest of the data shown in Figs. 2–4, we start from atomic samples in the three-dimensional harmonic dipole trap.

To measure the temperature of atoms or molecules (for example, Fig. 3b), we release them into a horizontally isotropic harmonic trap for a quarter of the trap period, which converts the particle distribution from real space to momentum space 31 . We extract the temperature T by fitting the momentum distribution with the condensate around zero momentum excluded using the Gaussian function $n(k_r) = n(0) \exp[-\hbar^2 k_r^2/(2mk_BT)]$, where k_r is the radial wavenumber and k_B is the Boltzmann constant.

Determination of Feshbach resonance position and width

To determine the position of the narrow *g*-wave Feshbach resonance in our system, we perform measurements of molecular binding energy at different offset magnetic fields using magnetic-field modulation spectroscopy^{32,33} and find the field value where the binding energy reaches zero.

We start with atomic BECs at 23 nK prepared at 19.5 G. Then, we quench the field to an offset value $B_{d,c}$ near the resonance and simultaneously modulate the field sinusoidally with an amplitude $B_{ac} = 5 \text{ mG}$ for 5 ms. We scan the modulation frequency and measure the spectrum of the remaining atom number. From the atom loss peak of the spectrum due to the conversion from atoms into molecules, we extract the resonant frequency that corresponds to molecular energy at an offset magnetic field $B_{d.c.}$ near the g-wave Feshbach resonance 31,32 (Extended Data Fig. 1). We have confirmed that the resulting peak position of atom loss is not sensitive to the modulation amplitude and modulation time. A linear fit to the data in Extended Data Fig. 1 gives the resonance posi $tion B_0 = 19.849(1)$ G where the molecular energy goes to zero. The slope of the linear fit gives the magnetic-moment difference between two bare atoms and one bare molecule as $\delta \mu = h \times 0.76(3)$ MHz G⁻¹, which is consistent with another work³⁰. We emphasize that for the narrow resonance we are using, the molecular energy quadratically approaches zero only within a small fraction of the resonance width. Our linear fit to the molecular energy data underestimates the resonance position by ~0.3 mG based on our calculation using the resonance width from the following scattering length measurements¹⁹. The systematic error

of our calibration of the absolute magnetic field is less than 20 mG. Throughout this work, we perform the magnetic-field calibration based on the same procedure to ensure a constant systematic error.

Next, we measure the s-wave scattering length near resonance to obtain the resonance width. Here the scattering length is inferred from the expansion of a quasi-2D BEC prepared with trap frequencies (ω_x , ω_y , ω_z) = $2\pi \times (11, 13, 895)$ Hz. During the expansion, the mean-field interaction energy is converted into kinetic energy. We first prepare the BEC at an initial magnetic field B_i = 20.481 or 19.498 G where the scattering is a_i . The column density distribution of atoms in the Thomas–Fermi regime is a_i

$$n(x,y) = \left[\mu - \frac{1}{2}m\omega_x^2 x^2 - \frac{1}{2}m\omega_y^2 y^2\right]/g_{2D},\tag{4}$$

where $g_{2\mathrm{D}}=(\hbar^2/m)\sqrt{8\pi}a_i/l_z$ is the coupling strength, $l_z=\sqrt{\hbar/m\omega_z}$ is the harmonic oscillator length in the tightly confined z direction and $\mu=\sqrt{g_{2\mathrm{D}}Nm\omega_x\omega_y/\pi}$ is the chemical potential determined by $g_{2\mathrm{D}}$, the total atom number N and the initial trap frequencies ω_x and ω_y in the horizontal plane. Then, we quench the magnetic field to a different value B_{f} where the scattering length is a_{f} and simultaneously switch off the harmonic trap in the horizontal plane. According to another work 35 , the dynamics of a BEC after release follow a simple dilation with scaling parameters $\lambda_x(t)$ and $\lambda_y(t)$, which determine the density distribution at time t as

$$n(x, y, t) = \frac{\mu - \frac{1}{2}m\omega_x^2 x^2 / \lambda_x^2(t) - \frac{1}{2}m\omega_y^2 y^2 / \lambda_y^2(t)}{g_{2D}\lambda_x(t)\lambda_y(t)},$$
 (5)

where the scaling parameters evolve according to

$$\ddot{\lambda}_{x}(t) = \frac{a_{f}}{a_{l}} \frac{\omega_{x}^{2}}{\lambda_{x}^{2}(t)\lambda_{y}(t)}$$

$$\ddot{\lambda}_{y}(t) = \frac{a_{f}}{a_{l}} \frac{\omega_{y}^{2}}{\lambda_{x}^{2}(t)\lambda_{x}(t)}.$$
(6)

We scan the magnetic field and measure the Thomas–Fermi radii $R_j = \sqrt{2\mu h_j^2(t)/m\omega_j^2}$ where j=x,y after 20 ms expansion. Eventually, we extract a_f based on its one-to-one correspondence to the Thomas–Fermi radii according to equation (6). The results are summarized in Extended Data Fig. 2 and we fit the scattering length data using the formula¹⁹

$$a(B) = a_{\text{bg}}[1 + \eta(B - B_0)] \left(1 - \frac{\Delta B}{B - B_0}\right),$$
 (7)

where we obtain the resonance width $\Delta B = 8.3(5)$ mG, the resonance position $B_0 = 19.861(1)$ G, the background scattering length on resonance $a_{\rm bg} = 163(1)a_0$ and the slope of the background scattering length $\eta = 0.31(2)$ G⁻¹. The background scattering length $a_{\rm bg}$ and slope η are consistent with ref. 36 and the resonance width ΔB is consistent with ref. 37, where a different method is used. The fitted resonance position deviates from that in the binding energy measurement by -10 mG, which we attribute to the heating of atoms near the resonance. The binding energy measurement, however, suffers less from the heating issue 32. Throughout this paper, we adopt the resonance position $B_0 = 19.849(1)$ G from the binding energy measurement.

Extraction of molecule oscillation frequency, atom loss rate and molecule formation rate

We use the following function to fit the data in the equilibration phase at 1 < t < 3 ms (Fig. 3) for the extraction of molecule oscillation frequencies³⁸:

$$N_{\rm m}(t) = N_{\rm m}(0) - \gamma_1 t + \Delta N_{\rm m} e^{-\gamma_2 t} \sin(\omega t + \phi), \tag{8}$$

where the fitting parameters are the molecule number $N_{\rm m}(0)$ extrapolated to time t=0, decay rates γ_1 and γ_2 , oscillation amplitude $\Delta N_{\rm m}$, oscillation frequency ω and phase ϕ . Here the two decay rates γ_1 and γ_2 characterize the decay of molecule number and damping of molecule oscillation amplitude, which are generally different.

For the data shown in Fig. 4, we fit the data at 0.3 < t < 3.0 ms using the function

$$N_{\rm m}(t) = {\rm e}^{-\gamma t} [N_{\rm m}(0) + \Delta N_{\rm m} \sin(\omega t + \phi)], \tag{9}$$

where we find that the single decay rate γ is enough to describe the data very well. For each fit, we subtract a delay time of 0.15 ms from time t due to the finite speed of our magnetic-field switch.

To prevent the fits from getting stuck in a local optimum, we vary the initial guess of frequency ω for the fits and use the result that has the minimum root mean square error.

For the atom loss rate measurement shown in Fig. 3c, we present example time traces of the averaged atomic density in the 2D flat-bottomed trap (Extended Data Fig. 3). Far from the resonance (Extended Data Fig. 3a,b), the atomic density decays slowly and we fit the data using

$$n_a(t) = n_a(0)e^{-\gamma_a t},$$
 (10)

where $n_a(0)$ is the initial atomic density and γ_a is the atom loss rate. The fit is applied to the data above half of the initial density.

Below and near the resonance (Extended Data Fig. 3c), we find that the density first decays rapidly and then settles around some equilibrium value before a slow decay kicks in at a timescale longer than 3 ms. In this case, we use the following fit function:

$$n_a(t) = n_a(0) \{ \theta(t_0 - t) + [(1 - s)e^{-\gamma_a(t - t_0)} + s]\theta(t - t_0) \},$$
 (11)

where t_0 is the time when the decay begins and s represents the fractional density that the system settles to after the initial fast decay. On the other hand, above and near the resonance (Extended Data Fig. 3d), the data are fit well by a single exponential decay (equation (10)).

Here we also provide the molecule formation rate measured near the resonance, complementary to the atom loss rate measurements shown in Fig. 3c (Extended Data Fig. 4).

Data availability

Source data are provided with this paper. All other data that support the plots within this paper are available from the corresponding author upon reasonable request.

Code availability

The codes for the analysis of data shown in this paper are available from the corresponding author upon reasonable request.

References

- 29. Hung, C.-L., Zhang, X., Gemelke, N. & Chin, C. Accelerating evaporative cooling of atoms into Bose-Einstein condensation in optical traps. *Phys. Rev. A* **78**, 011604 (2008).
- Chin, C. et al. Observation of Feshbach-like resonances in collisions between ultracold molecules. *Phys. Rev. Lett.* 94, 123201 (2005).
- Zhang, Z. Coherent Dynamics and Reactions in Atomic and Molecular Bose-Einstein Condensates (The Univ. Chicago, 2022).

- 32. Thompson, S. T., Hodby, E. & Wieman, C. E. Ultracold molecule production via a resonant oscillating magnetic field. *Phys. Rev. Lett.* **95**, 190404 (2005).
- 33. Lange, A. D. et al. Determination of atomic scattering lengths from measurements of molecular binding energies near Feshbach resonances. *Phys. Rev. A* **79**, 013622 (2009).
- Hung, C.-L., Zhang, X., Gemelke, N. & Chin, C. Observation of scale invariance and universality in two-dimensional Bose gases. *Nature* 470, 236–239 (2011).
- 35. Castin, Y. & Dum, R. Bose-Einstein condensates in time dependent traps. *Phys. Rev. Lett.* **77**, 5315–5319 (1996).
- 36. Berninger, M. et al. Feshbach resonances, weakly bound molecular states, and coupled-channel potentials for cesium at high magnetic fields. *Phys. Rev. A* **87**, 032517 (2013).
- Mark, M. J., Meinert, F., Lauber, K. & Nagerl, H.-C. Mott-insulator-aided detection of ultra-narrow Feshbach resonances. SciPost Phys. 5, 055 (2018).
- 38. Claussen, N. R. et al. Very-high-precision bound-state spectroscopy near a ⁸⁵Rb Feshbach resonance. *Phys. Rev. A* **67**, 060701 (2003).

Acknowledgements

We thank P. Julienne, K. Levin, D. Mazziotti, D. DeMille and K.-K. Ni for helpful discussions. We thank K. Patel and L. Weiss for carefully reading the paper. We thank J. Jachinowski for experimental assistance and carefully reading the paper. This work was supported by the National Science Foundation under grant nos. PHY1511696 and PHY-2103542 and by the Air Force Office of Scientific Research under award no. FA9550-21-1-0447. Z.Z. is supported by the Grainger Graduate Fellowship. S.N. acknowledges support from the Takenaka Scholarship Foundation.

Author contributions

Z.Z. and S.N. performed the experiments and analysed the data. Z.Z. built the theoretical model. K.-X.Y. contributed to the discussion of the results. C.C. supervised the work. All authors contributed to the writing of the paper.

Competing interests

The authors declare no competing interests.

Additional information

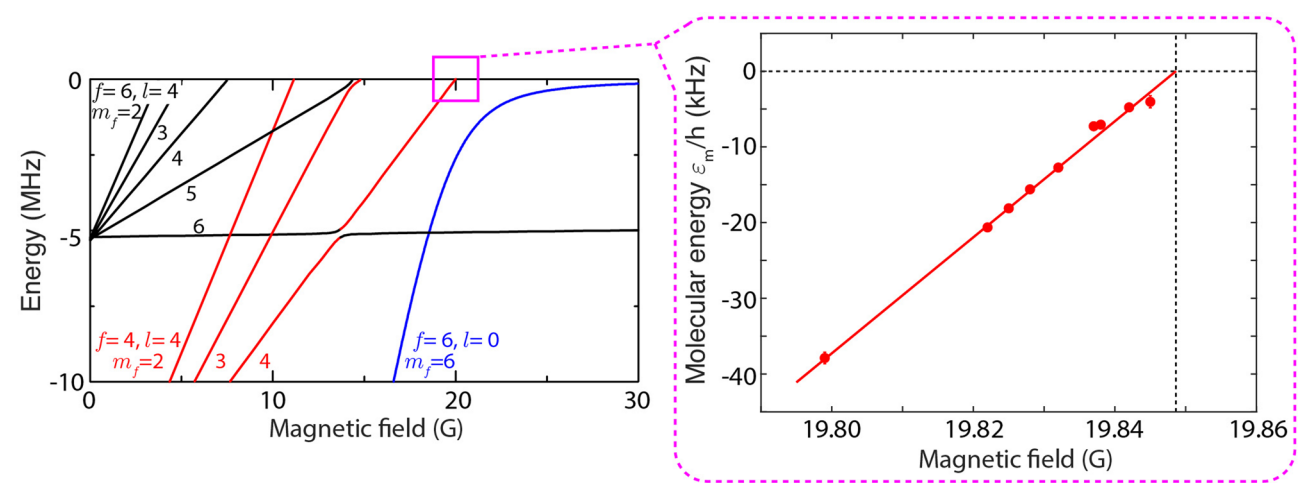
Extended data is available for this paper at https://doi.org/10.1038/s41567-023-02139-8.

Supplementary information The online version contains supplementary material available at https://doi.org/10.1038/s41567-023-02139-8.

Correspondence and requests for materials should be addressed to Cheng Chin.

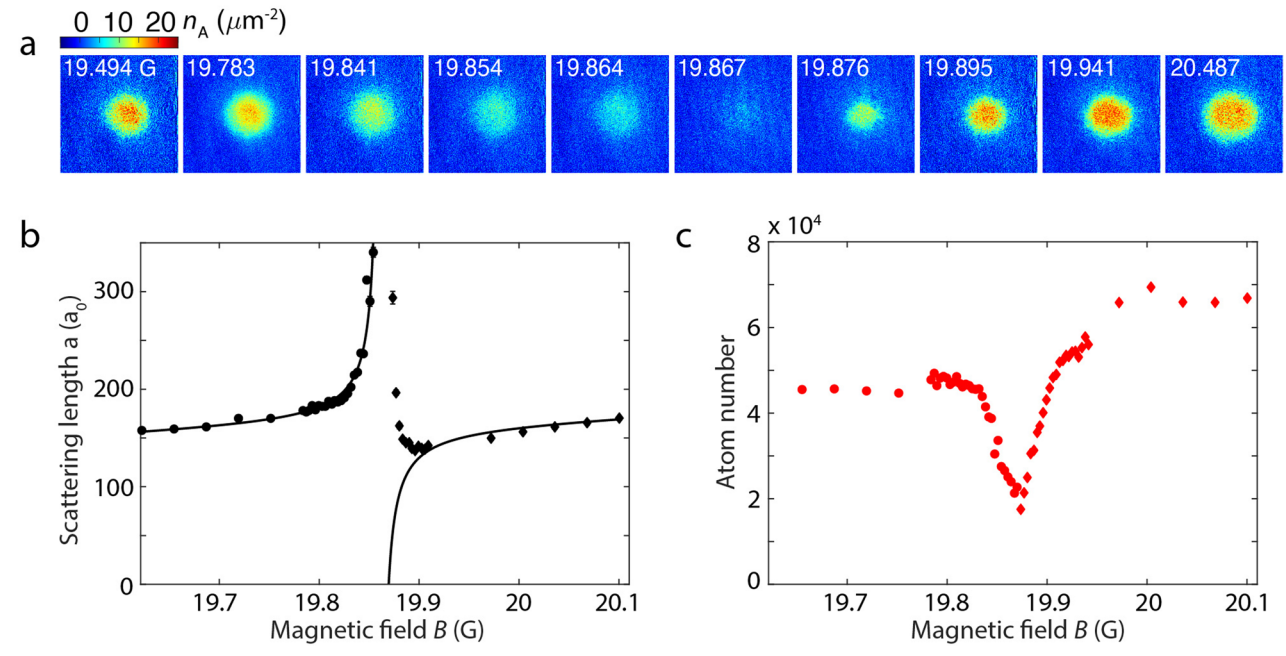
Peer review information *Nature Physics* thanks the anonymous reviewers for their contribution to the peer review of this work.

Reprints and permissions information is available at www.nature.com/reprints.



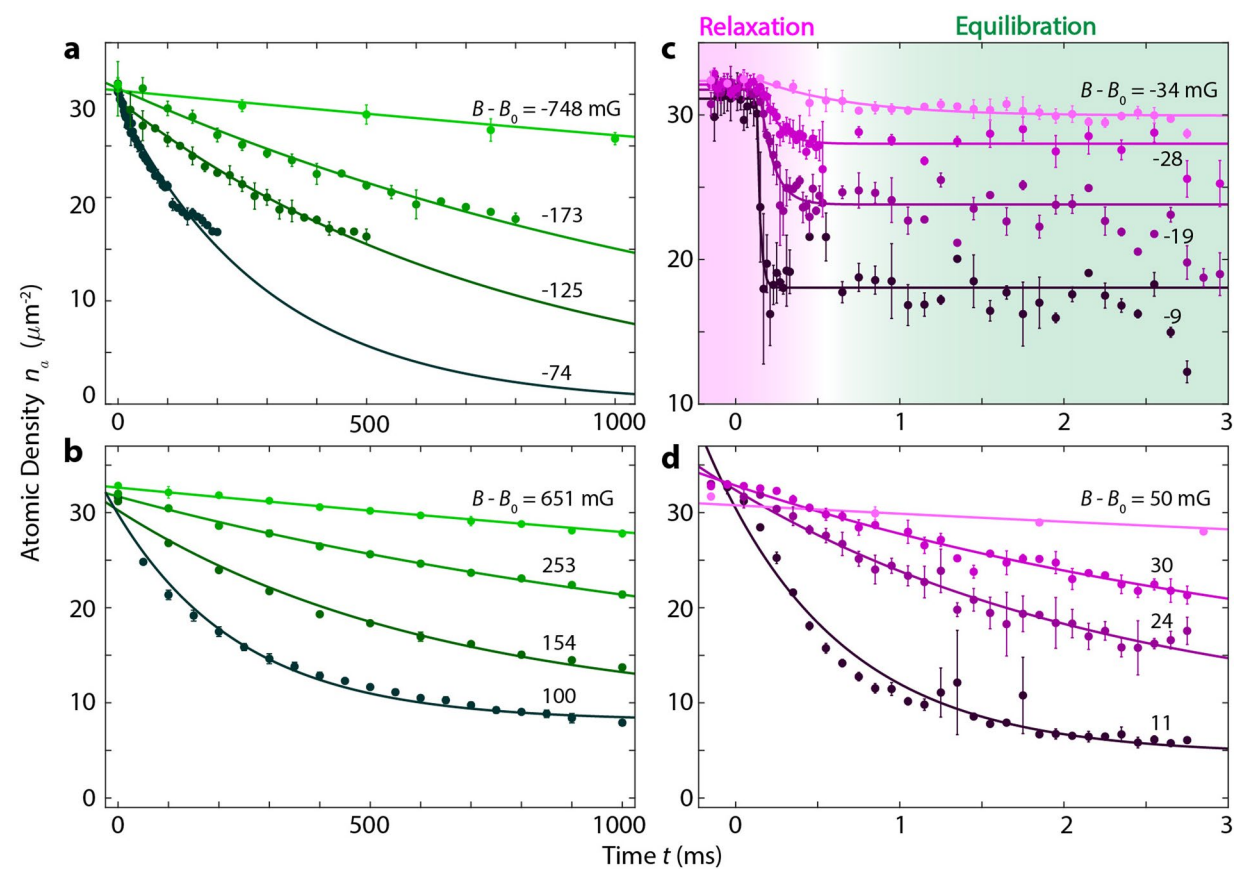
Extended Data Fig. 1|Bound state energy diagram for cesium atoms in the hyperfine ground state $|F=3,m_{\rm F}=3\rangle$ and molecular energy measurement near the g-wave Feshbach resonance around 20 G using modulation spectroscopy. a, Energy diagram for Cs₂ molecular states close to the atomic

scattering continuum adapted from Fig. 22 in Ref. 19. **b**, Molecular energy ε_m obtained from modulation spectroscopy at different offset magnetic fields. The solid line is a linear fit which reaches 0 at B_0 = 19.849(1) G.



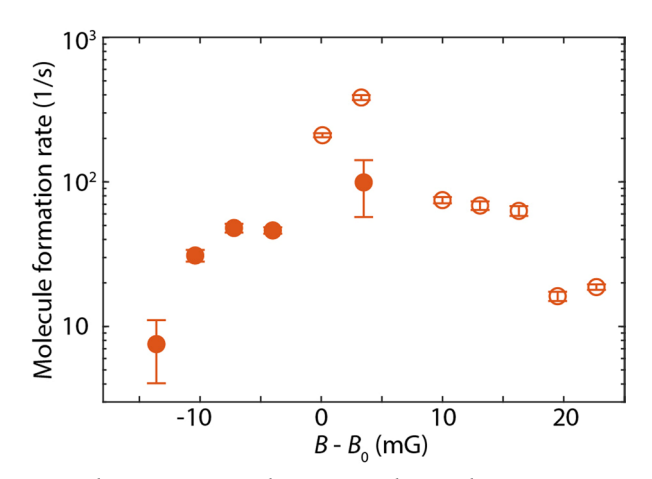
Extended Data Fig. 2 | **Scattering length measurement near the narrow g-wave Feshbach resonance by time-of-flight. a**, Atomic density distributions after 20 ms time-of-flight at different magnetic fields near the Feshbach resonance. The images with $B < 19.865 \ G \ (B > 19.865 \ G)$ come from initial BECs prepared below (above) the Feshbach resonance. **b**, Scattering length extracted from the Thomas-Fermi radii in the time-of-flight images, see text.

The circular (diamond) data points come from initial BECs prepared below (above) the resonance. The solid line is a fit to the data excluding the points at 19.858G < B < 19.909G based on Eq. (7), from which we obtain the resonance width $\Delta B = 8.3(5)$ mG. The points at 19.855G < B < 19.909G are excluded because of the heating effect near the resonance. **c**, Total atom number extracted from the time-of-flight images.



Extended Data Fig. 3 | Examples of atomic density evolution in a 2D flat-bottomed optical potential for the data presented in Fig. 3c. For data below the resonance, BECs are initially prepared at 19.5 G and magnetic field is quenched to values between 0.05 and 1G (panel a) and between 5 and 50 mG (panel c) below the resonance. Relaxation and equilibration phases are marked

with different background colors in panel ${\bf c}$. For data above the resonance, BECs are initially prepared at 20.4 G and magnetic field is quenched to values between 0.1 and 1 G (panel ${\bf b}$) and between 10 and 50 mG (panel ${\bf d}$) above the resonance. Solid lines are fits for extracting the atom loss rates, see text.



 $\textbf{Extended Data Fig. 4} | \textbf{Molecule formation rate near the resonance complementary to the atom loss rate measurements in Fig. 3c.} \\ \textbf{Solid (empty) circles represent samples prepared below (above) the resonance.} \\$